Journal of Chromatography A 1770 (2026) 466735

Contents lists available at ScienceDirect

Journal of Chromatography A

journal homepage: www.elsevier.com/locate/chroma

Overcoming challenges in LC separation of oxysterols through guided design space modelling: A comparison of three stationary phases

Andrea Castellaneta [a,*], Ilario Losito [a,b,*], Claudio Crisau [a], Arnold Zöldhegyi [c], Zuzana Hrušovská [c], Hans-Jürgen Rieger [c], Imre Molnár [c], Tommaso R.I. Cataldi [a,b]

[a] Dipartimento di Chimica, Università degli Studi di Bari Aldo Moro, Via Orabona 4, 70126 Bari, Italy
[b] Centro Interdipartimentale SMART, Università degli Studi di Bari Aldo Moro, via Orabona 4, 70126 Bari, Italy
[c] Molnár Institute for Applied Chromatography, Schneeglöckchenstraße 47, 10407 Berlin, Germany

ARTICLE INFO

Keywords:
Oxysterols
DryLab®
Analytical design space modelling
Reversed-phase liquid chromatography
High-resolution mass spectrometry

ABSTRACT

Liquid chromatography–mass spectrometry (LC–MS) is an attractive alternative to GC–MS for oxysterol (OS) analysis, as it eliminates the need for chemical derivatization. However, in-source fragmentation during electrospray ionization (ESI) or atmospheric pressure chemical ionization (APCI), usually adopted for LC-MS analysis of OS, may lead to the generation of isomeric ions from non-isomeric precursors. This prevents a complete unambiguous identification along the MS dimension and makes chromatographic separation a fundamental step. In this work, analytical design space modelling empowered by a software-based modelling tool (DryLab®) was employed to optimize the reversed-phase LC separations of ten clinically relevant OS, including isomeric ring-oxidized and side chain-oxidized sterols. Three stationary phases, octadecyl (C18), cyanopropyl (ES-CN), and pentafluorophenyl (F5), were compared in terms of separation efficacy, using HPLC columns of identical geometry (150 × 2.1 mm, 2.7 μm) packed with core–shell particles. Gradient steepness, column temperature, and composition of the organic modifier (mixture of methanol and acetonitrile) in the mobile phase were selected as critical method parameters for successive construction of the design spaces on the selected stationary phases. All the resulting optimized methods resolved positional isomers and diastereomers, excepting 25(R/S)-26-hydroxycholesterol epimers. The C18 stationary phase (at 52 °C) offered high selectivity but demanded the longest run times (ca. 80 min). ES-CN (at 50 °C) and F5 (at 25 °C) stationary phases enabled faster effective runs (< 45 min), with ES-CN also reducing retention/chemical artifacts that are presumably triggered by π-π binding interactions with the stationary phase.

1. Introduction

After being considered simply as intermediates in bile acid biosynthesis [1,2], oxysterols (OS) were found to be involved in the inhibition of sterol biosynthesis and the activity of 3-hydroxy-3-methylglutaryl coenzyme-A reductase (HMG-CoA) in cultured mammalian cells [3,4]. The subsequent extensive research efforts evidenced their role as signaling molecules in various biosynthetic pathways, as well as possible disease-related biomarkers [2,5,6].

OS are defined as oxidized derivatives of cholesterol and its biosynthetic precursors, including 7-dehydrocholesterol (DHC) and desmosterol [2,5]. As depicted in Fig. 1, both enzymatic and non-enzymatic oxidation processes contribute to the introduction of oxygen-based functionalities (e.g., hydroxyls, epoxides, ketones) into the cholesterol backbone [7], generating OS. The C7 position is recognized as the most reactive towards radical initiators such as hydroxyl and hydroperoxyl radicals, due to its allylic character [8,9]. As shown in Scheme S1, the resulting 7-cholesteryl radical can further react with oxygen in the reaction medium, generating 7-hydroxycholesterol and 7-hydroperoxycholesterol epimers, which can be further converted in a more stable oxidation product, i.e., 7-ketocholesterol (7-KC) [9,10]. 7-KC has been reported to increase cell membrane permeability and induce apoptosis [9,11], and also to be associated with an increased risk of vascular diseases due to facilitated atherogenesis [9,12]. Indeed, it was recognized as the most abundant OS in atherosclerotic plaques, followed by 7-hydroxycholesterol, 5,6-epoxycholesterol isomers and 3β, 5α,6β-cholestantriol [13]. Free 7-KC can be stereospecifically reduced to 7β-hydroxycholesterol (7β-HC) by 11β-hydroxysteroid dehydrogenase

* Corresponding authors at: Dipartimento di Chimica, Italy.
E-mail addresses: andrea.castellaneta@uniba.it (A. Castellaneta), ilario.losito@uniba.it (I. Losito).

https://doi.org/10.1016/j.chroma.2026.466735
Received 28 November 2025; Received in revised form 21 January 2026; Accepted 22 January 2026
Available online 23 January 2026
0021-9673/© 2026 Elsevier B.V. All rights are reserved, including those for text and data mining, AI training, and similar technologies.

type1 (11β-HSD1) [9,14,15], whereas its epimer, 7α-hydroxycholesterol (7α-HC), and 25(*R*)-26-hydroxycholesterol (25(*R*)-26-HC) are generated via the enzymatic oxidation of cholesterol by cholesterol 7α-hydroxylase (CYP7A) and sterol-27-hydroxylase (CYP27A1). These OS represent the first intermediates of the neutral (7α-HC) and acidic (25(*R*)-26-HC) pathways of bile acid biosynthesis [16].

Conversely to 7α-HC and other ring-oxidized forms of cholesterol (i.e., 7-KC, 7β-HC, cholesterol epoxides (EC) and 3β,5α,6β-cholestantriol (CT)), the formation of side-chain OS, including 25(*R*)-26-HC, 24(*S*)-hydroxycholesterol (24(*S*)-HC), and 25-hydroxycholesterol (25-HC), cannot be triggered by ROS, but is exclusively catalyzed by specific enzymes, most of which belonging to the cytochrome P450 family [1,5]. Side-chain OS are involved in fine tuning cholesterol metabolism [17,18], with 24(*S*)-HC playing a pivotal role in the brain tissue [19,20], where alterations of its levels have been related with the progression of several neurodegenerative pathologies, including Parkinson's, Alzheimer's, and Huntington's diseases [21,22]. Similarly to 24-HC, 26-HC can cross the blood-brain barrier (BBB); however, 26-HC exerts deleterious effects on neuronal cells, including cytotoxicity, impairment in neuronal morphology, and alteration of synaptic plasticity [23,24]. An increased amount of 26-HC was found in the brain of patients affected by Alzheimer's disease [25] and in the plasma of patients affected by hereditary spastic paraplegia type 5 (SPG5) [26]. Notably, the inhibition of CYP27A1 (i.e., the enzyme responsible for the conversion of cholesterol in 26-HC) has been suggested as a preventive therapeutical approach to restore the neural function and reduce the risk of dementia [27]. Some OS are also known to play a role in the immune system, with 25-hydroxycholesterol (25-HC) being produced by macrophages as a response to bacterial and viral infections [28–30]. OS have been also reported to be involved in malignancies such as breast, prostate, colon, and bile duct cancer [31] and to play an important role in the Hedgehog (HH) signalling pathway. The latter is critical in processes like embryonic development, tissue homeostasis, chemoattraction and synapse formation; thus its irregularities may be associated with congenital disorders and cancer [32].

The comprehensive understanding of the multifaceted biological role of OS is hindered by several challenges in their identification and quantification. OS are generally present in trace amounts in cells, tissues, and biological fluids, thus mass spectrometry combined with chromatographic separation has been widely exploited for their characterization [33,34]. In this context, liquid chromatography - mass spectrometry (LC-MS) has emerged as a suitable alternative to GC–MS, as it avoids potential artifacts related to the derivatization procedures required for GC separations. However, a major drawback of LC–MS is the formation of isomeric ions from non-isomeric OS due to in-source fragmentation occurring during typical ionization processes adopted for LC-MS (ESI, APCI). The observation of similar fragmentation pathways for different OS also complicates their selective identification by tandem MS (MS/MS). Hence, the optimization of the LC separation remains crucial to ensure robust and reliable OS analysis.

For the first time, this study introduced chromatography-based analytical Design Space modelling to optimize and compare the separation of 10 clinically relevant OS: 24(*S*)-HC, 25-HC, 25(*R*)-26-HC, 25(*S*)-26-HC, CT, 7α-HC, 7β-HC, 7-KC, 5α,6α-EC, and 5β,6β-EC. The investigation compared the performance of the octadecyl (C18) stationary phase, widely employed for LC separations of OS, with pentafluorophenyl (F5) and cyanopropyl (ES-CN) ones, both applied for the first time to the RPLC separation of OS. Conventional HPLC columns sharing identical geometrical formats (column length, internal diameter, and particle morphology/size) were employed. Key separation parameters, namely, gradient steepness, column temperature, and ternary composition of the mobile phase, were systematically investigated through multidimensional Design-of-Experiment (DoE) modelling based on the DryLab® suite (Molnár Institute, Berlin, Germany). DryLab® enables reliable prediction of chromatographic outcomes — including retention times, peak resolution, and overall separation profiles — across a wide range of conditions that would be impractical to explore experimentally within a reasonable timeframe [35–37]. These predictive outcomes are used to generate color-coded resolution maps, which illustrate the dependency of the critical resolution (Rs,crit, defined as the resolution of the closest eluting peak pair) on selected Design Space parameters [35–37]. This approach facilitates the rapid identification of separation conditions that meet or exceed predefined resolution thresholds. Additionally, the software's gradient editor module allows for the evaluation of more complex gradient profiles (e.g., multi-step gradients), offering further opportunities to enhance separation performance.

In the present study, chromatographic conditions enabling the separation of all target OS in the LC domain were successfully identified from a limited number (12) of preliminary experiments involving different combinations of three parameters, namely, column temperature (T) and gradient steepness (tG), that are generally recommended for evaluation, as they have consistently demonstrated a strong influence on separation selectivity [36], and composition of the organic modifier (tC)

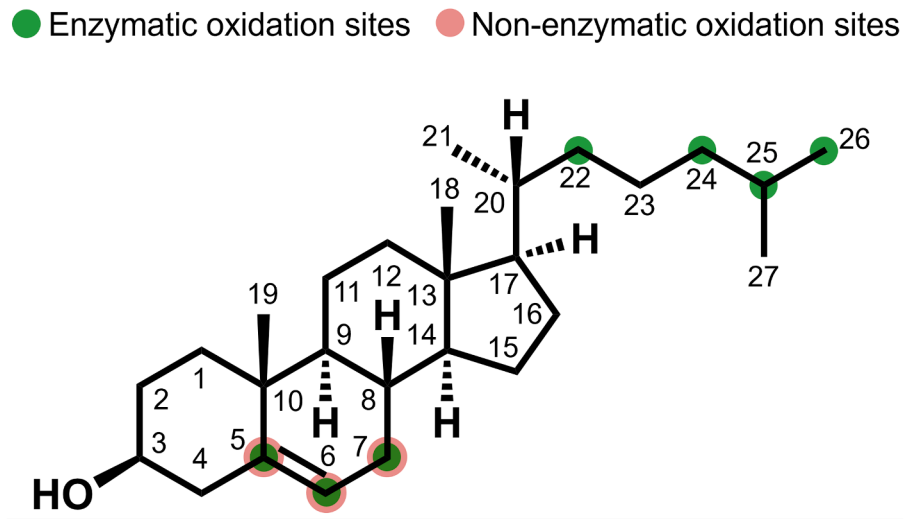


Fig. 1. Chemical structure of cholesterol, highlighting the oxidation sites leading to the formation of major oxysterols, including those investigated in this study (see Figure S1). The color-coded circles distinguish enzyme-specific oxidation sites (green) from those that can be also targeted by reactive oxygen species (red). The figure also displays the conventional atom numbering of the cholesterol backbone.

in the mobile phase.

An excellent agreement was observed between predicted and experimental retention times, thus validating the accuracy and reliability of the model-facilitated approach. This enhanced the critical comparison of the separation dynamics across the three stationary phases, revealing their respective strengths and limitations in OS analysis.

2. Materials and methods

2.1. Chemicals

LC-MS grade acetonitrile, methanol, and water (used for reversed-phase HPLC separations), along with LC-MS grade formic acid (used both as a mobile phase additive and co-adjuvant for electrospray ionization) were purchased from Merck (Milan, Italy). The analytical standards of 24(*S*)-hydroxycholesterol, 25-hydroxycholesterol, 25(*R*)-26-hydroxycholesterol, 25(*S*)-26-hydroxycholesterol, 3β,5α,6β-cholestantriol, 7α-hydroxycholesterol, 7β- hydroxycholesterol, 7-ketocholesterol, 5α,6α-epoxycholesterol, and 5β,6β-epoxycholesterol were purchased from Cayman Chemicals (Ann Arbor, USA).

2.2. LC-MS instrumentation and operating conditions

LC-MS analyses were performed using a platform implementing an Ultimate 3000 HPLC quaternary chromatographic system, including a Diode Array Detector (DAD) and a Q Exactive high-resolution quadrupole-Orbitrap mass spectrometer (Thermo Fisher, West Palm Beach, CA, USA). The chromatographic column effluent was transferred first into the DAD cell and then into the Heated ElectroSpray Ionization (HESI) interface (Thermo Fisher, West Palm Beach, CA, USA) mounted on the mass spectrometer. Reversed-phase liquid chromatography (RPLC) separations were performed using three different HPLC columns, supplied by Supelco (Bellefonte, USA): Ascentis® Express 90 Å C18 (octadecyl), Ascentis Express HPLC column 90 Å ES-CN (cyanopropyl), and Ascentis Express HPLC column 90 Å F5 (pentafluorophenyl). The columns shared identical length (15 cm), internal diameter (2.1 mm), and dimensions of the packing spherically porous (core-shell) particles (2.7 μm). In all cases, a 5 μL injection volume was adopted. The OS subjected to chromatographic separation were dissolved into ethanol, each at a 10 μg/mL concentration.

The parameters of the HESI interface and of the ion optics of the Q-Exactive spectrometer adopted during LC-MS analyses (and also for direct infusion analyses) were set as follows: sheath gas flow rate: 35 a.u.; auxiliary gas flow rate: 15 a.u.; spray voltage: 3.5 kV; capillary temperature: 320 °C; S-lens RF level: 50; Probe heater temperature: 40 °C. The Q Exactive mass spectrometer operated at its maximum resolving power (140,000 at *m/z* 200) for *full scan* experiments. *Full-scan* Fourier Transform mass spectra (FTMS) were acquired in a 300–500 *m/z* interval setting the Automatic Gain Control (AGC) level as 1×10^6, and the maximum injection time as 100 ms. Fourier Transform tandem mass spectra (FTMS/MS) were acquired after the collision-induced dissociation of the precursor ion in the higher-energy collisional dissociation (HCD) cell implemented in the Q Exactive mass spectrometer, using a normalized collision energy (NCE) of 30 units, an AGC level set to 2×10^5, and a maximum injection time of 100 ms. The isolation window for precursor ions was set as 1 *m/z* unit and FTMS/MS spectra were acquired at a resolving power of 70,000 units at *m/z* 200. The mass spectrometer was calibrated on alternate days by infusing, at a 5 μL/min flow rate, calibration solutions provided by the instrument manufacturer for both negative and positive polarity acquisitions. As a result, a mass accuracy always better than 5 ppm was achieved.

In addition to mass spectrometric detection, UV–Vis absorption was employed for the detection of OS after RPLC separations. UV–Vis spectra were acquired in the range 190–800 nm using the DAD included in the Ultimate3000 instrumentation and setting the bunch width as 1 nm, the data collection rate as 1 Hz and the response time as 10 s.

2.3. Design space modelling for oxysterols: experimental plan and details

As schematically represented in the experimental cube shown in Figure S2, the combination of two column temperatures (T), two gradient steepness values (tG), and three organic modifier compositions (tC) in the mobile phase resulted in 12 scouting experiments. These were performed on each of the three HPLC stationary phases under comparison (C18, ES-CN, and F5) to generate the input data required for the DryLab® suite. Although the use of ammonium salts was proposed to support ESI ionization of OS [38], in this study formic acid (FA) 0.1 % v/v was selected as the mobile phase additive to co-adjuvate the ESI ionization in positive-ion mode, and to avoid solubility issues, especially when pure acetonitrile was exploited as the organic modifier for some of the input runs. In addition, the distinctive in-source fragmentation patterns triggered by the FA-mediated protonation of OS (vide infra) were exploited for the identification of each chromatographic peak in the exploratory runs. Indeed, accurate peak identification and precise definition of system volumes are essential prerequisites for constructing reliable retention models. In the present case, the time shift arising from gradient delay—commonly referred to as dwell volume (V_D)— was estimated for the Ultimate 3000 HPLC system following the measurement protocol recommended by J.W. Dolan [39] and found to be equal to 936 μL.

The simultaneous UV and MS detection was employed to verify that the elution of all OS occurred in the time range of the linear gradient (see Figure S3). In particular, this precondition was verified in two short gradient run conditions (lower tG value), where temperature and tC conditions best inhibit (see point #9 of the experimental cube in Figure S2) or promote (see point #3 of the experimental cube in Figure S2) the elution of the analytes from the HPLC column. Suitable gradient range (start-end %B) conditions enabling the elution of all OS were achieved by modulating both the starting percentage of the organic modifier in the mobile phase and the lower gradient steepness (tG) value.

The 12 scouting experiments runs were performed in a time-efficient sequence, as previously proposed by Rácz et al. [40]: the first six experiments were conducted at low temperature, followed by the remaining six runs at high temperature. To minimize the time required for column conditioning and solvent reservoir exchanges, changes in gradient steepness (tG) were prioritized over variations in the organic modifier composition (tC). Accordingly, the numerical convention adopted in Figure S2 was followed, resulting in the run order: input condition no. 1, 2, 5, 6, 9, 10, followed by 3, 4, 7, 8, 11, and 12. Each sample injection was preceded by the injection of a blank sample, i.e., pure solvent sample under identical chromatographic conditions to ensure proper column equilibration.

3. Results and discussion

3.1. In-source fragmentation of oxysterols: a challenge for MS-based identification

For many Δ^5 steroids and sterols, protonation in ESI and APCI ion sources causes extensive in-source fragmentation processes, mainly consisting in consecutive water neutral losses, which reduce remarkably the detectability of the $[M + H]^+$ ion signal [41]. This behavior was confirmed by the ESI(+)-FTMS spectra collected for the OS considered in the present study upon direct infusion-MS analysis of their solutions (Fig. 2), with the signal due to the $[M + H]^+$ ion prevailing only for 7-ketocholesterol (vide infra). The similarity of ESI(+)-FTMS spectra observed for structurally different OS, including 3β,5α,6β-cholestantriol and 5,6-epoxycholesterol isomers (Figs. 2A–2C), could be explained by in-source fragmentation mechanisms shown in Scheme S2. Extensive in-source fragmentation, resulting in one or two water losses, was also

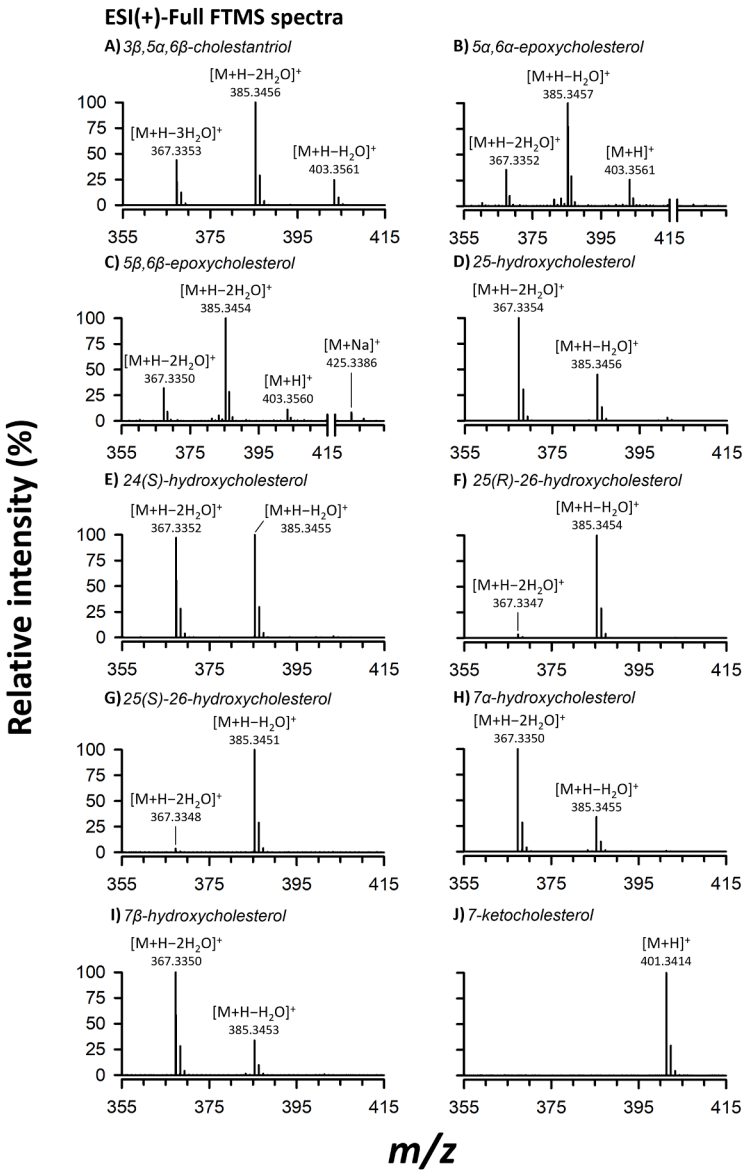


Fig. 2. ESI(+)-FTMS spectra acquired in Full MS scan mode after the direct infusion of 10 oxysterol standard solutions prepared in 1:1 methanol/acetonitrile mixtures containing formic acid 0.1 % v/v. Except for 7-ketocholesterol, extensive in-source fragmentation of protonated oxysterols generated isomeric ions even from non-isomeric compounds. In some cases, distinctive intensity ratios of the main FTMS signals could be observed.

observed for OS with the additional hydroxyl group on the side chain, such as 25-hydroxycholesterol (25-HC), 24-hydroxycholesterol (24-HC), and 26-hydroxycholesterol (26-HC) (Figs. 2D-2G) and is explained in detail by Scheme S3. Although the in-source fragmentation dynamics of hydroxyl groups in 7-hydroxycholesterol (7-HC), displayed in Scheme S4A, differ significantly from those discussed for 25-HC, their epimers displayed nearly indistinguishable ESI(+)-FTMS spectra (Figs. 2D, 2H, and 2I). As for 25-HC, the signal of the protonated form (*m/z* 403.3571) was absent, in accordance with the formation of stabilized carbocations after water elimination (see Scheme S4A). Conversely, as mentioned before, 7-ketocholesterol (7-KC) uniquely preserved its $[M + H]^+$ ion during the ESI process (Fig. 2J). This feature might be explained considering a predominant protonation on the oxo group, yielding a resonance-stabilized carbocation (Scheme S4B).

Table S1 summarizes the key features of OS ionization discussed above, highlighting that MS-based identification alone is highly challenging, even with high-resolution instruments, without adequate chromatographic separation. The DryLab®-assisted development of an effective LC separation strategy was thus pursued in this study as a crucial step for reliable OS analysis without derivatization. Notably, previous studies showed that the sensitivity and selectivity of ESI-MS detection for OS can be improved through hydroxyl group esterification with nitrogen-containing organic acids susceptible to protonation [42–44]. Derivatization with Girard reagents, which introduce a permanent positive charge via formation of a pyridine-containing hydrazone after enzymatic oxidation of the C3 hydroxyl group (common to all OS), was also investigated by Griffiths and coworkers [45]. It is worth noting that multiple isomers might be generated in case of incomplete derivatization reactions or when Girard reagents are employed [2], thus potentially increasing the complexity of OS analysis from a chromatographic point of view. Nonetheless, optimization strategies similar to the one explored in the present study for non-derivatized OS, might be applicable successfully also to their derivatized counterparts.

As detailed in Section S1, the comparison of the relative ion intensities in ESI(+)-FTMS spectra of LC-separated OS with those described in this section was central to the peak-tracking process for each scouting chromatogram, required before using DryLab®. This evaluation was particularly critical when peaks related to different OS

partially co-eluted, requiring deconvolution of composite chromatographic bands (see equations in Section S1).

3.2. Optimization of oxysterols separation on the octadecyl (C18) stationary phase

C18 columns are widely employed for the separation of native OS. The retention on the C18 stationary phase is mainly influenced by the position of additional oxygen atom(s) in the side chain rather than in the ring system [34]. In fact, sterol interaction with this stationary phase was shown to be primarily governed by the side chain [46,47]. Consequently, cholesterol oxidations occurring on the side chain usually result in lower retention compared to those on the steroidal backbone.

While the separation of ring- and side chain-oxidized OS is readily achievable with C18 HPLC columns, the resolution of epimers (e.g., 7α-HC and 7β-HC) and side-chain OS isomers (e.g., 25-HC and 24(*S*)-HC) remains a major challenge. To improve selectivity, several authors have tested different mobile phase compositions (typically consisting in water, acetonitrile, methanol, and isopropanol mixtures) and column temperatures (10–50 °C) [38,48–50]. A notable improvement in OS separation was recently achieved in the UHPLC regime by Della Valle et al. [51]. However, none of the previous studies achieved full separation of all compounds relevant to this work. We therefore attempted to improve separation by building upon the method reported by McDonald et al. [38]. This served as a reasonable reference point, as the method represents one of the most powerful analytical approaches for separating underivatized OS, along with other sterols and secosteroids, in human plasma. It is based on a typical microbore column packed with core-shell particles (150 × 2.1 mm, 2.6 μm), offering high efficiency and resolution. In our case, a similar C18 column was used but operated at a lower flow rate (0.25 vs. 0.5 mL/min), thus facilitating the direct interfacing with the HESI source of the mass spectrometer and the potential achievement of better MS sensitivity, which could be a critical issue, due to the low concentrations often expected for some OS. At the same time, the flow reduction enabled keeping the column backpressure below 400 bars, thus well beyond the maximum limit (600 bars) indicated by the manufacturer for the adopted core-shell packing. For similar reasons, since methanol- and acetonitrile-based hydro-organic mixtures exhibit lower viscosity, thus determining lower column backpressures, isopropyl alcohol was replaced accordingly in the mobile phase. The composition of the organic modifier (tC) was one of the three parameters subjected to subsequent modelling optimization, with three levels (see Figure S2) being explored during input runs: 0, 50 and 100 % methanol (B2) in acetonitrile (B1). The mobile phase was obtained as a mixture of water and the organic modifier (OM), both spiked with 0.1 % of formic acid to promote HESI ionization of oxysterols. A simple linear gradient was applied for modelling input runs (see Figure S2), starting from 70 % organic modifier to facilitate OS elution. A shallow gradient (0.6 % OM increase/min) was set for the shorter runs (see experiments no. 1,5,9,3, 7,11 in Figure S2), each lasting 50 min. Although a 1:3 ratio between short and long gradients is generally recommended [52], we set the lowest gradient slope at 0.375 %/min to ensure that total run time did not exceed 80 min. Temperature was the third factor selected for the optimization and was tested at two levels, i.e. 25 °C and 55 °C, consistently with the software-recommended 30 °C temperature range [52]. Working at temperatures below 25 °C was not considered due to concerns about column temperature control and increased solvent viscosity, particularly in the presence of high methanol content in the organic modifier.

During the separation optimization process the main focus was on 9 of the 10 oxysterols relevant to this study, namely 25-HC, 24(*S*)-HC, 25(*R*)-26-HC, 25(*S*)-26-HC, CT, 7α-HC, 7β-HC, 5β,6β-EC, and 5α,6α-EC. As previously discussed, these species are difficult to distinguish by MS alone. The tenth oxysterol, 7-KC, was excluded as it can be selectively monitored via the *m/z* 401.3414 channel. The outcome of each of the 12 input separations performed on the C18 column for the 9 oxysterols is graphically displayed in Figures S4-S15.

As expected, side chain-oxidized OS (25-HC, 24-HC, 25(*R*)-26-HC, 25(*S*)-26-HC) were eluted before ring OS (7α-HC, 7β-HC, 5β,6β-EC, and 5α,6α-EC) with CT eluting between the two groups. The two epimeric epoxides (5α,6α-EC and 5β,6β-EC) were well resolved under all conditions, whereas the epimers of 26-HC could not be separated, owing to their structural similarity. Separation of the 7-HC epimers and the remaining side-chain OS depended strongly on both temperature and OM composition. 7α-HC and 7β-HC were partially resolved when pure methanol was adopted as the OM and the separation was performed at 55 °C (Figures S14 and S15). An acceptable separation of 25-HC and 24-HC from 26-HC epimers was obtained in scouting run no.6 (Figure S9). At this selected input condition, pure acetonitrile (tC = 0 %) was exclusively used as the organic modifier, in combination with an extended gradient time (tG = 80 min) and elevated temperature ($T = 55$ °C). The elution order was 25-HC → 26-HC (co-eluting epimers) → 24-HC. Notably, the two 7-HC epimers were not separated under the same conditions. Interestingly, the increasing methanol in the OM drastically influenced the selectivity for the side chain-oxidized OS — in particular, the shift of the 24-HC peak towards the 25-HC, passing through the 26-HC peak.

Based on the outcome of scouting runs, it was evident that resolving the 7-HC epimers on the C18 column required a high methanol content and a relatively high temperature. Conversely, acetonitrile was necessary to separate side-chain OS. Therefore, an optimal balance of methanol and acetonitrile was needed to position 24(*S*)-HC between 25-HC and the 26(R/S)-HC epimers. These intuitive observations were further supported and refined by optimal operating conditions identified within the modelled Design Space. The software recommended $T = 51.9$ °C, tC=71 % (i.e., 71 % CH_3OH in CH_3CN), and the adoption of a two-step gradient to reach a critical resolution (Rs,crit) of 1.35 units. The detailed operating conditions are provided in Table 1. The comparison between the modelled and verification experiment is shown in Fig. 3, which also includes a 3D color-coded Design Space with the two-step linear gradient. In this case, red regions are the representation of Rs values higher than 1.2. The transition from red to yellow and green indicates increasing peak overlap, ultimately leading to coelution (Rs,crit = 0) in the blue regions. Despite the adjusted gradient program, the accuracy in retention time prediction of the model was always higher than 96 % (Table S2). Moreover, 97 % accuracy was calculated for the resolution between the 7-HC epimers, i.e., the model-identified critical peaks. However, contrary to expectations, the verification results revealed that 25-HC and 24(*S*)-HC constituted the actual least-resolved peak pair—-though still with a resolution greater than 1.2 units. These discrepancies may stem from robustness issues related to the instrument-delivered gradient program and could potentially be mitigated by employing high-pressure solvent delivery systems. Nevertheless, as evident from the chromatograms in Fig. 3, the primary limitation of the developed method on the C18 column was not the separation performance of the target oxysterols, but rather the overall run time of 1 hour and 20 min. To address this, a presumably less retentive cyanopropyl stationary phase was selected as a potential alternative.

3.3. Optimization of OS separation on the cyanopropyl (ES-CN) stationary phase

To date, cyano-bonded stationary phases have been applied to OS separation only in normal-phase liquid chromatography (NPLC) methods [53,54], with NPLC-APCI-MS successfully employed for the separation of 12 OS, including some of those relevant to this study [53]. However, NPLC is associated with well-known drawbacks, such as limited compatibility between mobile phase composition and ESI-based LC-MS coupling [34]. Furthermore, the use of more toxic organic solvents compared to those usually adopted in reversed-phase liquid chromatography (RPLC) raises concerns regarding operator safety and solvent disposal.

Table 1
Optimized chromatographic conditions developed in this study for the separation of a mixture of selected oxysterols using octadecyl (C18), cyanopropyl (ES-CN), and pentafluorophenyl (F5) HPLC columns (150 x 2.1 mm, packed with 2.7 μm core-shell particles). Binary elution gradients were based on water (solvent A) and an organic modifier represented by a mixture of methanol and acetonitrile (solvent B), both spiked with formic acid (0.1 %v/v) to enhance the MS detection of OS. The table lists additional data, like solvent consumption, column temperature and the maximum backpressure value measured during the chromatographic run. The duration of the run does not include the amount of time required for column cleaning/re-equilibration. In case of partial peak overlap, parameters required to calculate the chromatographic resolution (i.e., peak position and standard deviation) were determined using the "Gaussian multiple peak fit" function provided by the Origin® 2021 software.

Column	*Solvent A*	Solvent B (organic modifier)	*Structure of the elution gradient*	*Duration*	*Solvent consumption(single run)*	*Column temperature*	*Maximum backpressure*	*Chromatographic resolution (observed)*
C18	H_2O + FA (0.1 % v/v)	CH_3OH (79 % v/v) + CH_3CN (21 % v/v) + FA (0.1 % v/v)	Two-stage linear gradient: 0.00 - 36.02 min: linear increase of %B from 71.4 % to 74.0 %; 36.02 – 80 min: linear increase of %B from 74.0 % to 91.4 %.	80 min	H_2O: 4.36 mL CH_3OH: 12.36 mL CH_3CN: 3.28 mL	51.9 °C	187 bar	≥ 1.20 ***Critical peak pair:*** 25-hydroxycholesterol and 24(*S*)-hydroxycholesterol
ES-CN	H_2O + FA (0.1 % v/v)	CH_3OH (82 % v/v) + CH_3CN (18 % v/v) + FA (0.1 % v/v)	Simple linear gradient: 0.00 – 44.00 min: linear increase of %B from 40.0 % to 59.6 %;	44 min	H_2O: 5.52 mL CH_3OH: 0.99 mL CH_3CN: 4.49 mL	50 °C	165 bar	≥ 1.04 ***Critical peak pair:*** 3β,5α,6β-cholestantriol and 24(*S*)-hydroxycholesterol
F5	H_2O + FA (0.1 % v/v)	CH_3OH (47 % v/v) + CH_3CN (53 % v/v) + FA (0.1 % v/v)	Simple linear gradient: 0.00 – 40.00 min: linear increase of %B from 55.0 % to 75.0 %;	40 min	H_2O: 3.50 mL CH_3OH: 3.10 mL CH_3CN: 3.4 mL	25 °C	250 bar	≥ 1.23 ***Critical peak pair:*** 25-hydroxycholesterol and 24(*S*)-hydroxycholesterol

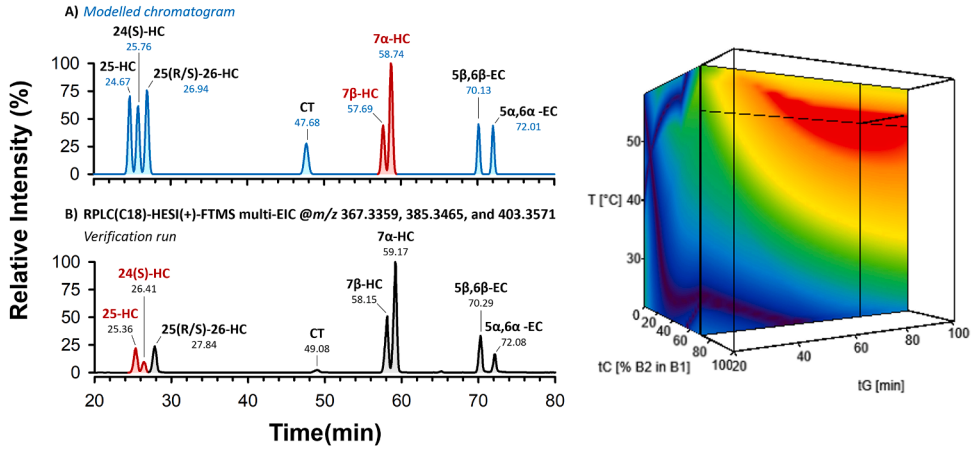


Fig. 3. Left) Comparison between the modelled chromatogram generated by DryLab® (panel A) and the corresponding RPLC(C18)-HESI(+)-FTMS verification chromatogram (panel B) obtained under the optimized separation conditions reported in Table 1. In both panels, the less resolved peaks (i.e., the peak pair corresponding to the critical resolution value) are highlighted in red. Modelled and observed retention time values are shown below each peak label to better evaluate the prediction accuracy of DryLab® (see Table S2 for details). Right) 3D color map illustrating the dependency of the critical resolution value on the three factors selected for the optimization. The map is based on the two-step linear gradient described in Table 1, with the color transition from blue to red indicating increasing critical resolution values.

To the best of our knowledge, this study represents the first attempt to use a cyano-bonded stationary phase for the RPLC separation of targeted OS. The separation on a cyanopropyl (ES-CN) HPLC column which shared the same geometric parameters as the previously used C18 column, was optimized with a similar chromatographic modelling work. Unlike C18, retention on the ES-CN stationary phase is presumed to be primarily governed by dipolar interactions, complemented by weak π–π binding and only moderate contributions from hydrophobic (dispersive) forces. Therefore, the percentage of the organic eluent for the 12 model input runs was reduced from 70 % to 40 % to lower the eluotropic strength of the mobile phase and prevent OS from eluting before the start of the effective gradient program. The duration of the short runs was reduced from 50 min to 30 min, with the higher tG value being increased from 80 min to 90 min to meet the software-required 1:3 ratio between lower and higher tG values [52]. The effects of T and tC were investigated using the same ranges and values adopted for the C18 columns. As for the C18 column, the optimization was focused on the separation of the 9 OS (25-HC, 24(*S*)-HC, 25(R/S)-26-HC, CT, 7α-HC, 7β-HC, 5α,6α-EC, and 5β,6β-EC) producing isomeric in-source product ions. The outcomes of the 12 scouting runs are displayed in Figures S16-S27.

As expected, side chain-oxidized OS eluted before ring-oxidized OS in all the 12 scouting runs, mirroring a similar elution pattern observed on the C18 column. However, even in this case the separation of the 26-HC epimers could not be achieved under any of the tested conditions. Additionally, the chromatographic separation of CT posed a new challenge as it tended to co-elute with side-chain OS in all scouting runs performed with the ES-CN column. In contrast, the separation of 7-HC epimers appeared to be more straightforward compared to the C18 stationary phase. A second challenge arose from the co-elution of the

two epoxy-cholesterol isomers, 5α,6α-EC and 5β,6β-EC, which were baseline-resolved on the C18 phase. Interestingly, the presence of methanol, combined with the elevated temperature (55 °C) used in scouting runs no. 7, 8, 11, and 12, resulted in a considerable baseline drift and peak distortion for both 5α,6α-EC and 5β,6β-EC peaks. Additionally, an unexpected peak appeared. The latter could not be attributed to any of the compounds in the standard mixture and was labelled as "U_{7HC}" in Figures S22, S23, S26, and S27. The corresponding full MS spectrum (not shown) exhibited two major peak signals at *m/z* 367.3351 and *m/z* 385.3457, with an intensity ratio similar to that observed for 25-HC and 7-HC epimers (see Figs. 2D, H, and I). As shown in Figure S28, the corresponding MS/MS spectra were similar to those of 7-HC epimers, but not to the spectrum of 25-HC. Whether U_{7HC} arose from a retention artifact involving 7-HC or from a chemical process remains unclear. Notably, the U_{7HC} peak was not observed in the scouting runs performed with the C18 column using pure methanol as the organic modifier at 55 °C. Therefore, it is likely that the ES-CN stationary phase played a major role in triggering its appearance. Furthermore, with increasing methanol concentration in the organic mobile phase, a progressive shift of the 24(*S*)-HC peaks towards the 25-HC was observed. Notably, this shift was also seen for CT, conversely to what occurred on the C18 column. Overall, balanced selectivity with the ES-CN phase was difficult to achieve, particularly for epoxy-cholesterol isomers and CT versus side-chain OS. For instance, while peaks 5α,6α-EC, and 5β,6β-EC were resolved in scouting run no.6 (see Figure S21), CT and 24(*S*)-HC co-eluted under the same operating conditions.

Starting from the outcome of the 12 input runs, the modelling software suggested the adoption of a linear gradient where the OM was increased from 40 % to 59.6 % in 44 min to achieve a Rs,crit value of 1.05. The software recommended as working conditions $T = 50$ °C and tC = 18 %. Further details are provided in Table 1.

The alignment between the modelled chromatogram at the optimized condition and the respective verification experiment is shown in Fig. 4. Despite the relatively high temperature, the verification chromatogram did not display the U_{7HC} peak or other artifacts, likely due to the limited amount of methanol in the mobile phase. Overall, the retention time modelling accuracy was high (99.5 %) except for CT, where it decreased to 98.3 %, most likely due to challenges in capturing the exact retention times of this peak during the tracking process (Table S3). CT was initially expected to partially co-elute with 25-HC. However, in the verification chromatogram, these two peaks were well resolved. Instead, a considerable overlap was observed between CT and 24(*S*)-HC. The calculated resolution for this pair was 1.04, which was lower than the observed resolution of 1.19 estimated for the anticipated critical peak pair, namely 5α,6α-EC and 5β,6β-EC.

Although average separation efficiency was generally lower than C18, the use of ES-CN column enabled a more compact elution of the targeted OS, resulting in a twofold reduction in total analysis time. In addition, a better resolution was achieved for 25-HC and 24(*S*)-HC, as well as for 7-HC epimers, whereas the separation between CT and 24(*S*)-HC and between 5α,6α-EC and 5β,6β-EC was less efficient. These observations indicate the ES-CN column as a promising alternative to C18 for the separation of OS. Nonetheless, improvements in terms of balance between separation efficiency and analysis time might be achieved by selecting a stationary phase representing a polarity compromise between C18 and ES-CN. Building on these results, the final stage of this work involved the use of a pentafluorophenyl (F5) column, geometrically equivalent to the C18 and ES-CN columns, for further optimization.

3.4. Optimization of OS separation on the pentafluorophenyl (F5) stationary phase

Due to the presence of rigid aromatic rings, introducing steric constraints that can be exploited to highlight potential differences in molecular shape (e.g., those arising from the different location of functional groups among regioisomers) the pentafluorophenyl (F5) stationary phase has been recently proposed as a suitable alternative to the C18 one for the separation of a wide range of sterols [55]. However, the interaction of native OS with the F5 moieties remains poorly investigated. An hybrid C18-F5 stationary phase, in which the pentafluorophenyl group is linked to the end of an octadecyl spacer, was mentioned by Roberg-Larsen *et al.* [56] as a potential tool for the separation of steroid-like molecules.

Dev *et al.* [57] employed a more conventional F5 stationary phase, where the pentafluorophenyl moiety was linked to the silica structure via a propyl spacer. This column was successfully applied for separating native OS and their sulfated derivatives. The authors adopted the same flow rate and a column geometry similar to that adopted in the C18 and ES-CN methods developed in the present study. However, it remained unclear whether their method could resolve OS epimers such as 7α-HC and 7β-HC.

Building on the promising separation possibilities of the F5 column, a similar optimization workflow was applied for the separation of targeted OS (25-HC, 24(*S*)-HC, 25(R/S)-26-HC, CT, 7α-HC, 7β-HC, 5α,6α-EC, and

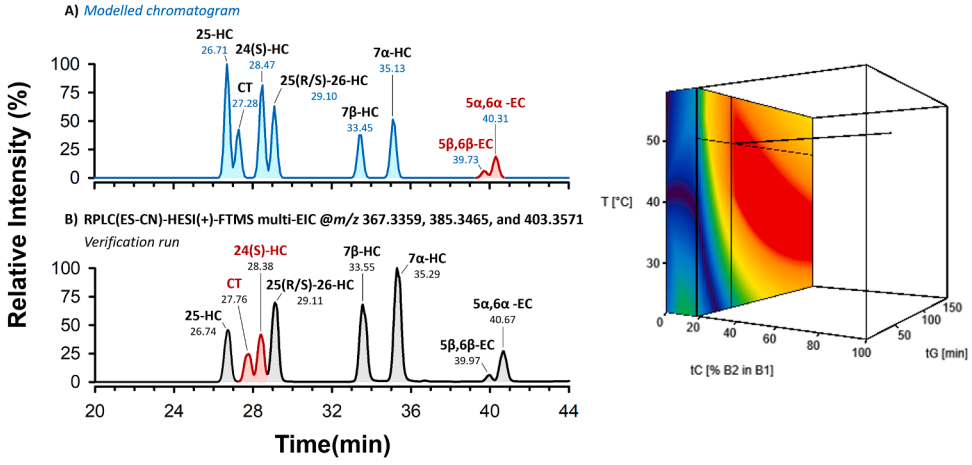


Fig. 4. Left) Comparison between the modelled chromatogram generated by DryLab® (panel A) and the corresponding RPLC(ES-CN)-HESI(+)-FTMS verification chromatogram (panel B) obtained under the optimized separation conditions reported in Table 1. In both panels, the less resolved peaks (i.e., the peak pair corresponding to the critical resolution value) are highlighted in red. Modelled and observed retention time values are shown below each peak label to better evaluate the prediction accuracy of DryLab® (see Table S2 for details). Right) 3D color map illustrating the dependency of the critical resolution value on the three factors selected for the optimization. The map is based on the two-step linear gradient described in Table 1, with the color transition from blue to red indicating increasing critical resolution values.

5β,6β-EC), and the results were compared with the C18 and ES-CN-based methods. To ensure consistency across the tested separation systems, the same column geometry and flow rate were maintained during the modelling input and subsequent optimization process.

As with the ES-CN stationary phase, interactions with the F5 phase are only moderately governed by dispersive forces. In order to fit to the linear gradient range, the starting proportion of the OM was set here to 45 % across the 12 exploratory runs. The duration of the short and long runs (40 min and 80 min, respectively) approximated the recommended 1:3 ratio [52]. A lower temperature limit of 30 °C was selected to prevent analytes from pre-eluting or post-eluting during the experiments. As previously mentioned, the software recommends a 30 °C gap between the two operating temperatures [52], yet the upper limit was set at 50 °C since this helped to avoid operating too close to the column supplier's maximum specified temperature of 60 °C.

As for C18 and ES-CN methods, the three tC levels tested in the exploratory runs were: pure acetonitrile, a 50 % v/v methanol/acetonitrile mixture, and pure methanol. The chromatograms achieved during the 12 exploratory runs with the F5 column are presented in Figures S29-S40.

Using pure acetonitrile as OM at 30 °C with the 80 min-long gradient enabled complete separation of nearly all analytes of interest, except 24(*S*)-HC and the two 26-HC epimers (Figure S30). As observed with both the C18 and ES-CN columns, 26-HC epimers could not be resolved under any exploratory condition. Raising the column temperature to 50 °C during acetonitrile-based runs adversely affected the separation, producing pronounced tailing for CT and 7β-HC peaks. The first four input runs revealed common traits across C18, ES-CN, and F5 stationary phases. In all cases, the elution order reflected the oxidation site: side chain OS eluted before ring-OS, with CT positioned between these two groups. This represented a substantial improvement over the ES-CN method, where CT partially co-eluted with 24(*S*)-HC. Like ES-CN, the F5 column yielded a more compact elution profile, enabling shorter analysis times compared to the C18 one. As observed with both C18 and ES-CN, the presence of methanol in the mobile phase shifted progressively 24(*S*)-HC towards the 25-HC peak. The complete separation between side chain OS (excluding the 26-HC epimers) was achieved when methanol was raised to 50 % in the OM at 30 °C. However, under these conditions, the U_{7HC} peak emerged, causing significant baseline distortion in the epoxy-cholesterol region, although their peaks remained well resolved (Figures S33 and S34).

As described in the previous section, a low-intensity U_{7HC} peak was observed when the separation with the ES-CN column was performed using pure methanol at 55 °C. The separation based on 100 % methanol with the F5 column resulted in a severe distortion of the baseline under the epoxy-cholesterols peaks already at 30 °C, along with the partial or complete co-elution between 5α,5α-EC and U_{7HC} (see Figures S37 and S38). Therefore, accurate peak tracking of ring OS was no longer feasible in the modelling input runs performed at 50 °C when methanol was included in the organic eluent. In contrast, peaks corresponding to side chain OS were consistently identified across all the 12 runs.

Based on the results described so far, it can be inferred that the use of relatively high temperatures in combination with methanol in the organic modifier led to distortion in peak position and shape during the separation of ring oxysterols on stationary phases capable of π–π interactions. It remains unclear whether these effects arose from alterations in the retention mechanism or from chemical reactions occurring during the chromatographic process. Importantly, the severity of distortion correlated positively with the π–π acceptor strength of the stationary phase, increasing markedly from ES-CN to F5.

Once the detrimental effect of high temperatures combined with the presence of methanol was recognized for the F5 column, the optimization of chromatographic conditions with the modelling tool was restricted to the tG x tC plane at fixed temperature, i.e., by considering only the modelling input runs no. 1,2,5,6,9, and 10 (see Figure S2). As suggested by the outcome of runs no. 1,2,5, and 6, the presence of methanol in the OM was unavoidable, as it improved separation of side-chain OS and epoxy-cholesterol isomers. Accordingly, DryLab® recommended the use of a tC = 47 % MeOH in ACN organic composition, along with the use of a simple linear gradient where the organic amount was increased from 55 % to 75 % in 40 min. Panels A and B in Fig. 5 compare the modelled chromatogram and the verification one obtained under the optimized conditions. In addition, the figure provides a color-coded 2D-map of the critical resolution as a function of tG and tC parameters, with column temperature fixed at 30 °C. The highest resolution values could be achieved for tC corresponding to almost equal percentages of methanol and acetonitrile. However, as evidenced in Fig. 5B, methanol induced the already mentioned distortion of the baseline beneath the two epoxy-cholesterol peaks. While accurate resolution could not be determined for this pair of peaks due to distortion, the corresponding isomers were visibly separated. Accurate resolution values were thus calculated for the remaining peak pairs in the verification run. The corresponding values are shown in Table S4 and compared with those predicted by the software. Table S4 also includes the comparison between the modelled and observed retention times, with modelling accuracy higher than 98 %. Based on the outcome of the modelling input runs performed with the F5 column, the reduction of the column temperature was expected to mitigate the extent of baseline distortion. Therefore, the verification run was repeated under the optimized conditions but with column temperature reduced from 30 °C to 25 °C (i.e., the laboratory working temperature). As shown in Fig. 5C, the arbitrary decrease of temperature by 5 °C was sufficient to noticeably reduce the extent of baseline alteration, although some distortion remained detectable. At the same time, separation of target OS was maintained with only some expected increase of their retention times. The operating conditions that led to the chromatogram reported in Fig. 5C are summarized in Table 1.

A final comparison of OS separations achieved with the three stationary phases is provided in Fig. 6, in which extracted ion chromatogram (EIC) traces for 7-ketocholesterol (7-KC) are also included. The figure emphasizes that all the developed methods effectively separated it from other sterols, although this is not a stringent requirement, since 7-KC can be distinctly monitored in the MS domain.

It is worth noting that the present study focused on a selected subset of the broad spectrum of known oxysterols and, therefore, it did not include certain species with recognized biochemical relevance. These comprise 4β-hydroxycholesterol (an endogenous CYP3A activity marker [58]), 22(*R*)- hydroxycholesterol (involved in neurosteroid biosynthesis [59]), 24S,25-epoxycholesterol (an important LXR ligand involved in cholesterol homeostasis [60]), as well as other cholesterol oxidized derivatives such as cholestenoic acids [61]. However, the developmental workflow described in this manuscript can be readily adapted to standard mixtures relevant to the specific biochemical context under investigation. Moreover, appropriate modifications of the operating flow, in combination with modified geometrical characteristics of the adopted columns, might enable a reduction of run times in contexts requiring higher sample throughputs.

4. Conclusions

The LC-ESI-MS analysis of 10 clinically relevant OS was successfully achieved using each of three stationary phase chemistries, namely C18, ES-CN, and F5, through method development and optimization guided by the DryLab® software, and focused on 9 species among them, oxidized either on the steroidal ring or on the side chain and exhibiting superimposable ESI ionization channels (i.e., *m/z* 367.3359, 385.3465, and 403.3571) due to in-source fragmentation. Starting from a set of 12 modelling input experiments, based on different combinations of column temperature (T), gradient time (tG), and methanol/acetonitrile organic modifier composition (tC), optimal chromatographic conditions were successfully achieved in all cases using software-based retention modelling, with separation of positional isomers, as well as

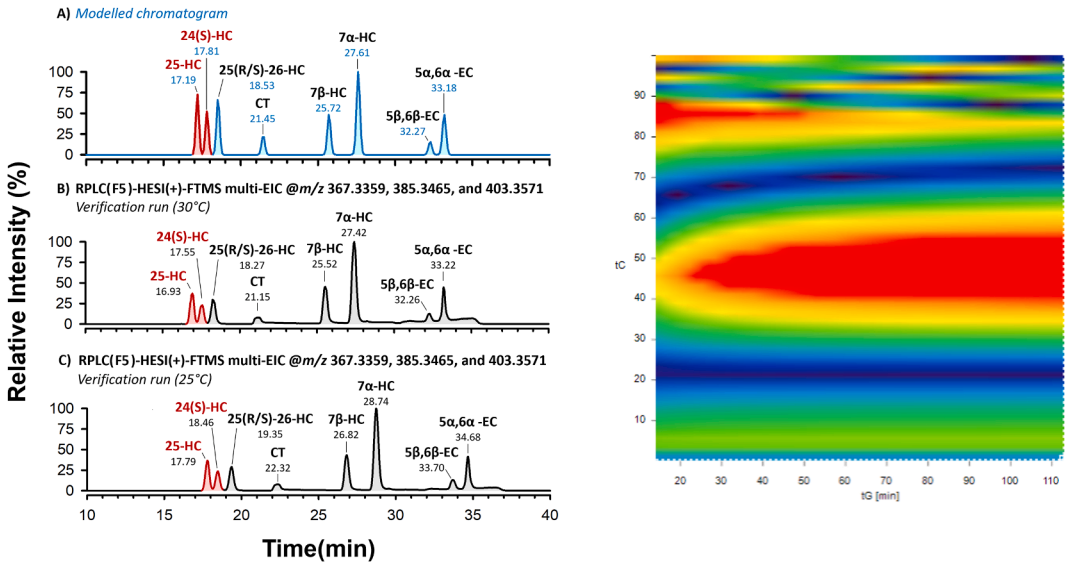


Fig. 5. Left) alignment between the modelled chromatogram generated by DryLab® (panel A) and the corresponding RPLC(F5)-HESI(+)-FTMS verification chromatogram (panel B) obtained under the separation conditions optimized for the F5 stationary phase. Right) 2D color map showing the dependency of the critical resolution value on the two factors selected for the optimization (tG and tC), with column temperature fixed at 30 °C. Panel C illustrates how decreasing column temperature from 30 to 25 °C under optimized conditions mitigate baseline artifacts in the time-range of epoxy-cholesterol elution caused by the presence of methanol in the mobile phase (see the text for details).

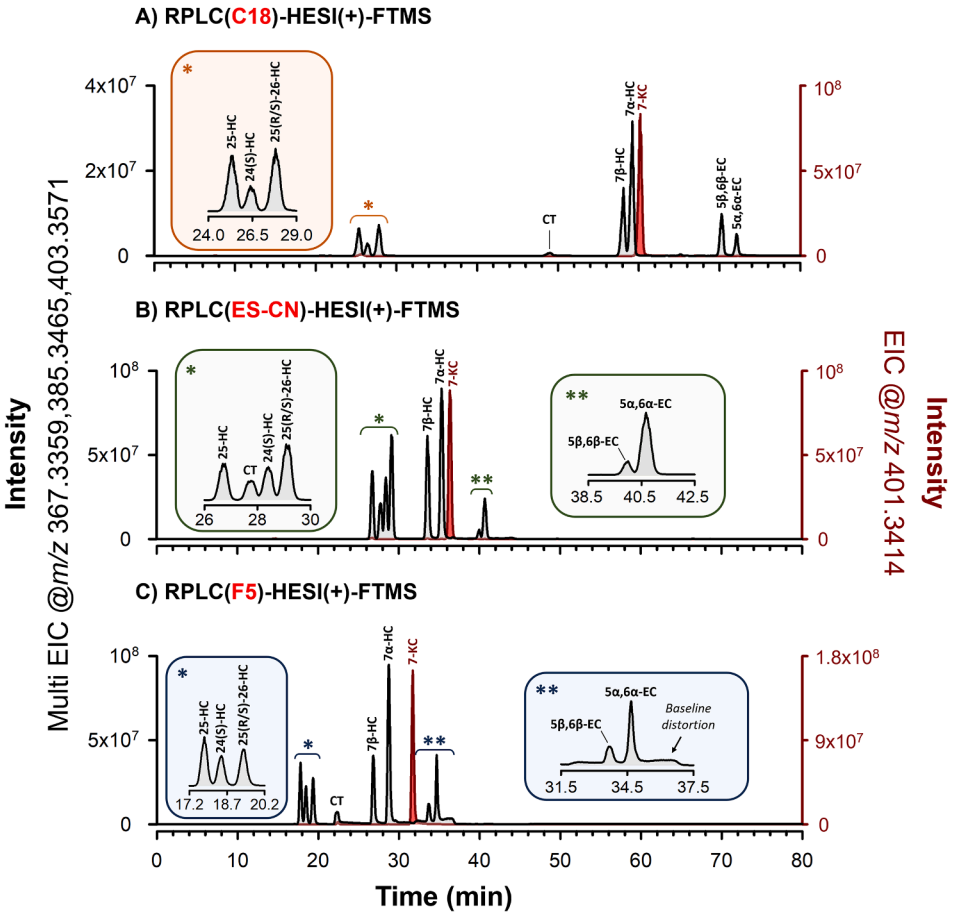


Fig. 6. RPLC—HESI(+)-FTMS extracted ion chromatograms obtained under the optimized conditions summarized in Table 1 for the separation of 10 oxysterols using C18 (panel A), ES-CN (panel B), and F5 (panel C) HPLC columns. In each panel, the EIC trace of the $[M + H]^+$ ion of 7-ketocholesterol (red line) is overlaid with the multiple EIC trace (black line) referring to the main ions generated by the protonation and the following in-source fragmentation of the other nine oxysterols. Ion currents were extracted using a 5 ppm-wide isolation window centred on the theoretical *m/z*value of each target ion. Insets report magnifications of retention time intervals in which peaks were closely spaced and/or minor baseline artifacts were present.

diastereomers differing in the spatial distribution of oxygen-based functionalities, with the only exception of 25(R/S)-26-HC epimers.

Due to the strong retention of ring-oxidized oxysterols, related to their unmodified, hydrophobic side chain, the C18 phase required the longest analysis times for an optimal separation, with the implementation of a two-step multilinear gradient required to tackle the hard challenge posed by the separation of highly retained 7-hydroxycholesterol epimers. In contrast, the more polar ES-CN and F5 stationary phases enabled similar separation results within shorter analysis times. Among these alternative phases, the ES-CN one provided the best compromise between analysis time and baseline artifacts observed when methanol and relatively high column temperatures were adopted during modelling input runs. On the other hand, the F5 phase enabled a neat separation of 3β,5α,6β-cholestantriol from side chain oxysterols.

Ultimately, this study demonstrated that chromatography-based modelling approaches can effectively rationalize method development, even for structurally similar oxysterol compounds. By minimizing the number of input experiments required to establish optimal conditions, satisfactory separation was already achieved in the LC dimension, thereby facilitating subsequent MS-based characterization and emphasizing the pros and cons of the application of each of the three stationary phases under study to complex oxysterol mixtures.

Funding sources

This research was financially supported by a PRIN 2022 PNRR project (project code P2022RW885), funded by the Italian *Ministero per l'Università e la Ricerca*.

CRediT authorship contribution statement

Andrea Castellaneta: Writing – original draft, Validation, Methodology, Investigation, Data curation, Conceptualization. **Ilario Losito:** Writing – review & editing, Validation, Supervision, Resources, Project administration, Methodology, Funding acquisition, Conceptualization. **Claudio Crisau:** Investigation, Data curation. **Arnold Zöldhegyi:** Writing – review & editing, Visualization, Validation, Investigation, Data curation. **Zuzana Hrušovská:** Visualization, Investigation, Data curation. **Hans-Jürgen Rieger:** Writing – review & editing. **Imre Molnár:** Writing – review & editing. **Tommaso R.I. Cataldi:** Writing – review & editing, Funding acquisition.

Declaration of competing interest

The authors declare that they have no known competing financial interests or personal relationships that could have appeared to influence the work reported in this paper.

Supplementary materials

Supplementary material associated with this article can be found, in the online version, at doi:10.1016/j.chroma.2026.466735.

Data availability

Data will be made available on request.

References

[1] W.J. Griffiths, Y. Wang, Oxysterols as lipid mediators: their biosynthetic genes, enzymes and metabolites, Prostaglandins Other Lipid Mediat. 147 (2020) 106381, https://doi.org/10.1016/j.prostaglandins.2019.106381.
[2] W.J. Griffiths, Y. Wang, Oxysterol research: a brief review, Biochem. Soc. Trans. 47 (2019) 517–526, https://doi.org/10.1042/BST20180135.
[3] A.A. Kandutsch, H.W. Chen, Inhibition of sterol synthesis in cultured mouse cells by 7alpha-hydroxycholesterol, 7beta-hydroxycholesterol, and 7-ketocholesterol, J. Biol. Chem. 248 (1973) 8408–8417. http://www.ncbi.nlm.nih.gov/pubmed/4797016.
[4] G.J. Schroepfer, Oxysterols: modulators of Cholesterol Metabolism and Other Processes, Physiol. Rev. 80 (2000) 361–554, https://doi.org/10.1152/physrev.2000.80.1.361.
[5] W. Luu, L.J. Sharpe, I. Capell-Hattam, I.C. Gelissen, A.J. Brown, Oxysterols: old Tale, New Twists, Annu. Rev. Pharmacol. Toxicol. 56 (2016) 447–467, https://doi.org/10.1146/annurev-pharmtox-010715-103233.
[6] F.A. de Freitas, D. Levy, C.O. Reichert, E. Cunha-Neto, J. Kalil, S.P. Bydlowski, Effects of oxysterols on immune cells and related diseases, Cells 11 (2022) 1251, https://doi.org/10.3390/cells11081251.
[7] M. Poirot, S. Silvente-Poirot, Cholesterol-5,6-epoxides: chemistry, biochemistry, metabolic fate and cancer, Biochimie 95 (2013) 622–631, https://doi.org/10.1016/j.biochi.2012.05.006.
[8] N.A. Porter, L. Xu, D.A. Pratt, Reactive sterol electrophiles: mechanisms of formation and reactions with proteins and amino acid nucleophiles, Chemistry (Easton) 2 (2020) 390–417, https://doi.org/10.3390/chemistry2020025.
[9] A. Anderson, A. Campo, E. Fulton, A. Corwin, W.G. Jerome, M.S. O'Connor, 7-Ketocholesterol in disease and aging, Redox Biol. 29 (2020) 101380, https://doi.org/10.1016/j.redox.2019.101380.
[10] L. Iuliano, Pathways of cholesterol oxidation via non-enzymatic mechanisms, Chem. Phys. Lipids 164 (2011) 457–468, https://doi.org/10.1016/j.chemphyslip.2011.06.006.
[11] R. Filomenko, C. Fourgeux, L. Bretillon, S. Gambert-Nicot, Oxysterols: influence on plasma membrane rafts microdomains and development of ocular diseases, Steroids 99 (2015) 259–265, https://doi.org/10.1016/j.steroids.2015.02.004.
[12] C.I. Seye, M.W.M. Knaapen, D. Daret, C. Desgranges, A.G. Herman, M.M. Kockx, H. Bult, 7-Ketocholesterol induces reversible cytochrome c release in smooth muscle cells in absence of mitochondrial swelling, Cardiovasc. Res. 64 (2004) 144–153, https://doi.org/10.1016/j.cardiores.2004.05.016.
[13] C. Helmschrodt, S. Becker, J. Schröter, M. Hecht, G. Aust, J. Thiery, U. Ceglarek, Fast LC–MS/MS analysis of free oxysterols derived from reactive oxygen species in human plasma and carotid plaque, Clin. Chim. Acta 425 (2013) 3–8, https://doi.org/10.1016/j.cca.2013.06.022.
[14] R.A.S. Schweizer, M. Zürcher, Z. Balazs, B. Dick, A. Odermatt, Rapid Hepatic Metabolism of 7-Ketocholesterol by 11β-Hydroxysteroid Dehydrogenase Type 1, J. Biol. Chem. 279 (2004) 18415–18424, https://doi.org/10.1074/jbc.M313615200.
[15] A. Vejux, D. Abed-Vieillard, K. Hajji, A. Zarrouk, J.J. Mackrill, S. Ghosh, T. Nury, A. Yammine, M. Zaibi, W. Mihoubi, H. Bouchab, B. Nasser, Y. Grosjean, G. Lizard, 7-Ketocholesterol and 7β-hydroxycholesterol: in vitro and animal models used to characterize their activities and to identify molecules preventing their toxicity, Biochem. Pharmacol. 173 (2020) 113648, https://doi.org/10.1016/j.bcp.2019.113648.
[16] W.M. Pandak, G. Kakiyama, The acidic pathway of bile acid synthesis: not just an alternative pathway, Liver Res. 3 (2019) 88–98, https://doi.org/10.1016/j.livres.2019.05.001.
[17] S. Gill, R. Chow, A. Brown, Sterol regulators of cholesterol homeostasis and beyond: the oxysterol hypothesis revisited and revised, Prog. Lipid Res. 47 (2008) 391–404, https://doi.org/10.1016/j.plipres.2008.04.002.
[18] B. Wang, P. Tontonoz, Liver X receptors in lipid signalling and membrane homeostasis, Nat. Rev. Endocrinol. 14 (2018) 452–463, https://doi.org/10.1038/s41574-018-0037-x.
[19] J.M. Dietschy, S.D. Turley, Thematic review series: brain Lipids. Cholesterol metabolism in the central nervous system during early development and in the mature animal, J. Lipid Res. 45 (2004) 1375–1397, https://doi.org/10.1194/jlr.R400004-JLR200.
[20] I. Björkhem, Rediscovery of Cerebrosterol, Lipids 42 (2007) 5–14, https://doi.org/10.1007/s11745-006-1003-2.
[21] V. Leoni, C. Mariotti, S.J. Tabrizi, M. Valenza, E.J. Wild, S.M.D. Henley, N. Z. Hobbs, M.L. Mandelli, M. Grisoli, I. Björkhem, E. Cattaneo, S. Di Donato, Plasma 24S-hydroxycholesterol and caudate MRI in pre-manifest and early Huntington's disease, Brain 131 (2008) 2851–2859, https://doi.org/10.1093/brain/awn212.
[22] V. Leoni, J.D. Long, J.A. Mills, S. Di Donato, J.S. Paulsen, Plasma 24S-hydroxycholesterol correlation with markers of Huntington disease progression, Neurobiol. Dis. 55 (2013) 37–43, https://doi.org/10.1016/j.nbd.2013.03.013.
[23] L. Schöls, T.W. Rattay, P. Martus, C. Meisner, J. Baets, I. Fischer, C. Jägle, M. J. Fraidakis, A. Martinuzzi, J.A. Saute, M. Scarlato, A. Antenora, C. Stendel, P. Höflinger, C.M. Lourenco, L. Abreu, K. Smets, M. Paucar, T. Deconinck, D.M. Bis, S. Wiethoff, P. Bauer, A. Arnoldi, W. Marques, L.B. Jardim, S. Hauser, C. Criscuolo, A. Filla, S. Züchner, M.T. Bassi, T. Klopstock, P. De Jonghe, I. Björkhem, R. Schüle, Hereditary spastic paraplegia type 5: natural history, biomarkers and a randomized controlled trial, Brain 140 (2017) 3112–3127, https://doi.org/10.1093/brain/awx273.
[24] P. Merino-Serrais, R. Loera-Valencia, P. Rodriguez-Rodriguez, C. Parrado-Fernandez, M.A. Ismail, S. Maioli, E. Matute, E.M. Jimenez-Mateos, I. Björkhem, J. DeFelipe, A. Cedazo-Minguez, 27-Hydroxycholesterol Induces Aberrant Morphology and Synaptic Dysfunction in Hippocampal Neurons, Cereb. Cortex 29 (2019) 429–446, https://doi.org/10.1093/cercor/bhy274.
[25] W.J. Griffiths, J. Abdel-Khalik, E. Yutuc, G. Roman, M. Warner, J.-Å. Gustafsson, Y. Wang, Concentrations of bile acid precursors in cerebrospinal fluid of Alzheimer's disease patients, Free Radic. Biol. Med. 134 (2019) 42–52, https://doi.org/10.1016/j.freeradbiomed.2018.12.020.
[26] R. Schüle, T. Siddique, H.-X. Deng, Y. Yang, S. Donkervoort, M. Hansson, R. E. Madrid, N. Siddique, L. Schöls, I. Björkhem, Marked accumulation of 27-hydroxycholesterol in SPG5 patients with hereditary spastic paresis, J. Lipid Res. 51 (2010) 819–823, https://doi.org/10.1194/jlr.M002543.

[27] M. Lam, N. Mast, I.A. Pikuleva, Drugs and scaffold that inhibit cytochrome P450 27A1 in vitro and in vivo, Mol. Pharmacol. 93 (2018) 101–108, https://doi.org/10.1124/mol.117.110742.
[28] D.R. Bauman, A.D. Bitmansour, J.G. McDonald, B.M. Thompson, G. Liang, D. W. Russell, 25-Hydroxycholesterol secreted by macrophages in response to Toll-like receptor activation suppresses immunoglobulin A production, Proc. Natl. Acad. Sci. 106 (2009) 16764–16769, https://doi.org/10.1073/pnas.0909142106.
[29] U. Diczfalusy, K.E. Olofsson, A.-M. Carlsson, M. Gong, D.T. Golenbock, O. Rooyackers, U. Fläring, H. Björkbacka, Marked upregulation of cholesterol 25-hydroxylase expression by lipopolysaccharide, J. Lipid Res. 50 (2009) 2258–2264, https://doi.org/10.1194/jlr.M900107-JLR200.
[30] M. Blanc, W.Y. Hsieh, K.A. Robertson, K.A. Kropp, T. Forster, G. Shui, P. Lacaze, S. Watterson, S.J. Griffiths, N.J. Spann, A. Meljon, S. Talbot, K. Krishnan, D. F. Covey, M.R. Wenk, M. Craigon, Z. Ruzsics, J. Haas, A. Angulo, W.J. Griffiths, C. K. Glass, Y. Wang, P. Ghazal, The transcription factor STAT-1 couples macrophage synthesis of 25-hydroxycholesterol to the interferon antiviral response, Immunity 38 (2013) 106–118, https://doi.org/10.1016/j.immuni.2012.11.004.
[31] A. Kloudova, F.P. Guengerich, P. Soucek, The role of oxysterols in human cancer, Trends Endocrinol. Metab. 28 (2017) 485–496, https://doi.org/10.1016/j.tem.2017.03.002.
[32] H. Roberg-Larsen, M.F. Strand, S. Krauss, S.R. Wilson, Metabolites in vertebrate hedgehog signaling, Biochem. Biophys. Res. Commun. 446 (2014) 669–674, https://doi.org/10.1016/j.bbrc.2014.01.087.
[33] W.J. Griffiths, J. Abdel-Khalik, P.J. Crick, E. Yutuc, Y. Wang, New methods for analysis of oxysterols and related compounds by LC–MS, J. Steroid Biochem. Mol. Biol. 162 (2016) 4–26, https://doi.org/10.1016/j.jsbmb.2015.11.017.
[34] I.H.K. Dias, S.R. Wilson, H. Roberg-Larsen, Chromatography of oxysterols, Biochimie 153 (2018) 3–12, https://doi.org/10.1016/j.biochi.2018.05.004.
[35] I. Molnár, H.-J. Rieger, K.E. Monks, Aspects of the "Design Space" in high pressure liquid chromatography method development, J. Chromatogr. A. 1217 (2010) 3193–3200, https://doi.org/10.1016/j.chroma.2010.02.001.
[36] J.W. Dolan, L.R. Snyder, T. Blanc, L. Van Heukelem, Selectivity differences for C18 and C8 reversed-phase columns as a function of temperature and gradient steepness, J. Chromatogr. A. 897 (2000) 37–50, https://doi.org/10.1016/S0021-9673(00)00851-7.
[37] A. Zöldhegyi, K. Horváth, R. Kormány, Revisiting column selectivity choices in ultra-high performance liquid chromatography–using multidimensional analytical design Spaces to identify column equivalency, J. Chromatogr. A. 1719 (2024) 464738, https://doi.org/10.1016/j.chroma.2024.464738.
[38] J.G. McDonald, D.D. Smith, A.R. Stiles, D.W. Russell, A comprehensive method for extraction and quantitative analysis of sterols and secosteroids from human plasma, J. Lipid Res. 53 (2012) 1399–1409, https://doi.org/10.1194/jlr.D022285.
[39] J.W. Dolan, Dwell volume revisited, LCGC North Am. 24 (2006) 458–466.
[40] N. Rácz, R. Kormány, J. Fekete, I. Molnár, Establishing column batch repeatability according to Quality by Design (QbD) principles using modeling software, J. Pharm. Biomed. Anal. 108 (2015) 1–10, https://doi.org/10.1016/j.jpba.2015.01.037.
[41] K.D. McCarty, F.P. Guengerich, Mass spectral analysis of sterols and other steroids in different ionization modes: sensitivity and oxidation artifacts, J. Am. Soc. Mass Spectrom. (2025), https://doi.org/10.1021/jasms.5c00099.
[42] A. Honda, K. Yamashita, T. Hara, T. Ikegami, T. Miyazaki, M. Shirai, G. Xu, M. Numazawa, Y. Matsuzaki, Highly sensitive quantification of key regulatory oxysterols in biological samples by LC-ESI-MS/MS, J. Lipid Res. 50 (2009) 350–357, https://doi.org/10.1194/jlr.D800040-JLR200.
[43] R. Sidhu, H. Jiang, N.Y. Farhat, N. Carrillo-Carrasco, M. Woolery, E. Ottinger, F. D. Porter, J.E. Schaffer, D.S. Ory, X. Jiang, A validated LC-MS/MS assay for quantification of 24(S)-hydroxycholesterol in plasma and cerebrospinal fluid, J. Lipid Res. 56 (2015) 1222–1233, https://doi.org/10.1194/jlr.D058487.
[44] Z. Pataj, G. Liebisch, G. Schmitz, S. Matysik, Quantification of oxysterols in human plasma and red blood cells by liquid chromatography high-resolution tandem mass spectrometry, J. Chromatogr. A. 1439 (2016) 82–88, https://doi.org/10.1016/j.chroma.2015.11.015.
[45] P.J. Crick, T.William Bentley, J. Abdel-Khalik, I. Matthews, P.T. Clayton, A. A. Morris, B.W. Bigger, C. Zerbinati, L. Tritapepe, L. Iuliano, Y. Wang, W. J. Griffiths, Quantitative charge-tags for sterol and oxysterol analysis, Clin. Chem. 61 (2015) 400–411, https://doi.org/10.1373/clinchem.2014.231332.
[46] V. Cinquepalmi, I. Losito, A. Castellaneta, C.D. Calvano, T.R.I. Cataldi, APCI-multistage mass spectrometry following liquid chromatography for selected 4-desmethyl-sterols and their deuterium-Labelled analogues unveils characteristic fragmentation routes for cholesterol and phytosterols identification, Rapid Commun. Mass Spectrom. 39 (2025), https://doi.org/10.1002/rcm.10039.
[47] V. Cinquepalmi, I. Losito, A. Castellaneta, C.D. Calvano, T.R.I. Cataldi, Diagnostic fragmentations of animal and fungal sterols/stanols obtained by APCI–tandem mass spectrometry: a route towards unknown free sterol identification, Metabolites 15 (2025) 674, https://doi.org/10.3390/metabo15100674.
[48] A.E. DeBarber, D. Lütjohann, L. Merkens, R.D. Steiner, Liquid chromatography–tandem mass spectrometry determination of plasma 24S-hydroxycholesterol with chromatographic separation of 25-hydroxycholesterol, Anal. Biochem. 381 (2008) 151–153, https://doi.org/10.1016/j.ab.2008.05.037.
[49] N.C. van de Merbel, K.J. Bronsema, M.W.J. van Hout, R. Nilsson, H. Sillén, A validated liquid chromatography–tandem mass spectrometry method for the quantitative determination of 4β-hydroxycholesterol in human plasma, J. Pharm. Biomed. Anal. 55 (2011) 1089–1095, https://doi.org/10.1016/j.jpba.2011.03.017.
[50] I.H.K. Dias, I. Milic, G.Y.H. Lip, A. Devitt, M.C. Polidori, H.R. Griffiths, Simvastatin reduces circulating oxysterol levels in men with hypercholesterolaemia, Redox Biol 16 (2018) 139–145, https://doi.org/10.1016/j.redox.2018.02.014.
[51] F.Della Valle, F. Eugelio, C. Merola, G. Caioni, F. Fanti, M. Mascini, A. Damiano, M. Amorena, M. Del Carlo, M. Sergi, D. Compagnone, Oxysterol fingerprinting via UPLC-APCI-MS/MS for monitoring developmental stages in the zebrafish model, J. Pharm. Biomed. Anal. 267 (2026) 117156, https://doi.org/10.1016/j.jpba.2025.117156.
[52] I. Molnár, K.E. Monks, From Csaba Horváth to Quality by Design: visualizing Design Space in Selectivity Exploration of HPLC Separations, Chromatographia 73 (2011) 5–14, https://doi.org/10.1007/s10337-011-1968-8.
[53] T. Saldanha, A.C.H.F. Sawaya, M.N. Eberlin, N. Bragagnolo, HPLC separation and determination of 12 cholesterol oxidation products in fish: comparative study of RI, UV, and APCI-MS detectors, J. Agric. Food Chem. 54 (2006) 4107–4113, https://doi.org/10.1021/jf0532009.
[54] C.H. Grün, S. Besseau, Normal-phase liquid chromatography–atmospheric-pressure photoionization–mass spectrometry analysis of cholesterol and phytosterol oxidation products, J. Chromatogr. A. 1439 (2016) 74–81, https://doi.org/10.1016/j.chroma.2015.12.043.
[55] C. Skubic, I. Vovk, D. Rozman, M. Križman, Simplified LC-MS method for analysis of sterols in biological samples, Molecules 25 (2020) 4116, https://doi.org/10.3390/molecules25184116.
[56] H. Roberg-Larsen, C. Vesterdal, S.R. Wilson, E. Lundanes, Underivatized oxysterols and nanoLC–ESI-MS: a mismatch, Steroids 99 (2015) 125–130, https://doi.org/10.1016/j.steroids.2015.01.023.
[57] S. Dev, A. Muchenditsi, A. Gottlieb, P. Deme, S. Murphy, K.L. Gabrielson, Y. Dong, R. Hughes, N.J. Haughey, J.P. Hamilton, S. Lutsenko, Oxysterol misbalance critically contributes to Wilson disease pathogenesis, Sci. Adv. 8 (2022), https://doi.org/10.1126/sciadv.adc9022.
[58] U. Diczfalusy, H. Nylén, P. Elander, L. Bertilsson, 4β-hydroxycholesterol, an endogenous marker of CYP3A4/5 activity in humans, Br. J. Clin. Pharmacol. 71 (2011) 183–189, https://doi.org/10.1111/j.1365-2125.2010.03773.x.
[59] A. Meljon, S. Theofilopoulos, C.H.L. Shackleton, G.L. Watson, N.B. Javitt, H.-J. Knölker, R. Saini, E. Arenas, Y. Wang, W.J. Griffiths, Analysis of bioactive oxysterols in newborn mouse brain by LC/MS, J. Lipid Res. 53 (2012) 2469–2483, https://doi.org/10.1194/jlr.D028233.
[60] A.J. Brown, 24(S),25-Epoxycholesterol: a messenger for cholesterol homeostasis, Int. J. Biochem. Cell Biol. 41 (2009) 744–747, https://doi.org/10.1016/j.biocel.2008.05.029.
[61] P.J. Crick, L. Beckers, M. Baes, P.P. Van Veldhoven, Y. Wang, W.J. Griffiths, The oxysterol and cholestenoic acid profile of mouse cerebrospinal fluid, Steroids 99 (2015) 172–177, https://doi.org/10.1016/j.steroids.2015.02.021.